Calculation of PWR Reactor Xenon Poisoning Using the Wigner-Seitz Approximation and Physics-Informed Neural Networks

Lucija Dasović
University of Zagreb, Faculty of Science, Department of Physics
Horvatovac 102a, 10000 Zagreb, Croatia
lucija.dasovic@student.pmf.hr

Mario Matijević
University of Zagreb Faculty of Electrical Engineering and Computing
Department of Applied Physics
Unska 3, 10000 Zagreb, Croatia
mario.matijevic@fer.hr

ABSTRACT

During the PWR reactor operation, fission products accumulate in the nuclear fuel giving an increase in the absorption of thermal neutrons, which reduces the reactor reactivity. This phenomenon, known as reactor poisoning, is primarily associated with the xenon ^{135}Xe and samarium ^{149}Sm isotopes, which reach their maximum concentration relatively quickly during the reactor operation. The biggest contribution to poisoning comes from the isotope ^{135}Xe due to its extremely large absorption cross section for thermal neutrons (about 3 million barns), so knowing its temporal concentration is essential for calculating the change in reactor reactivity. In order to assess the influence of a particular radionuclide on the reactor's reactivity, it is necessary to solve its Bateman equations, which describe the balance of the processes of creation and disappearance of nuclides in the neutron field. The analytical solution to ^{135}Xe temporal concentration includes the thermal neutron utilization factor (*f*-factor), which will be explicitly modelled in this paper. The heterogeneous unit fuel cell will be modelled using the neutron diffusion theory in cylindrical geometry, within the Wigner-Seitz approximation. The obtained analytical and numerical results of the *f*-factor, ^{135}Xe concentrations, and resulting changes in reactor reactivity will serve as input data for training physics-informed neural network (PINN) algorithms. This test-case from reactor physics will examine PINNs applicability and level of their numerical predictive accuracy.

Keywords: *xenon, PWR reactor poisoning, thermal neutron utilization factor, Wigner-Seitz approximation, physics-informed neural networks*

1 INTRODUCTION

The fission fragments and their many decay products accumulate during the course of nuclear reactor operation, with nuclides ^{135}Xe and ^{149}Sm having the most profound effect due to exceptionally large absorption cross section for thermal neutrons. These nuclei will decrease the neutron multiplication factor k_{eff} by lowering the thermal neutron utilization *f*-factor, so common name for them is "neutron poisons". The concentration of fission-product poisons will be affected by a change in the neutron flux, resulting in the reactor reactivity change. The ^{135}Xe isotope can be formed directly and indirectly in fission and can be removed via radioactive decay and neutron capture. With specific reactor power level, the xenon concentration will reach an equilibrium value.

During the reactor shut down, the production of ^{135}Xe is coming from the parent ^{135}I decay, but the main mechanism of removal by neutron capture is lost, resulting in concentration increase to a maximum before finally decreasing. The neutron flux is thus determining the equilibrium and maximum xenon concentration which effects reactivity. The analyses show how ^{235}U fission can produce fission products of over 200 different nuclides. Half of them can be disregarded with small impact on reactivity, while other half is divided in two parts:

a) nuclides which reach relatively quickly their maximum concentration during reactor startup, or better to say they go quickly into the saturation (^{135}Xe and ^{149}Sm)
b) all nuclides which reach a saturation value during a long time (or not at all) and their effect is considered summarily.

The reactivity change due to fission-product poisons can be expressed as

$$\Delta\rho = \rho' - \rho\,, \tag{1}$$

where the first and second term relate to poisoned and non-poisoned reactor, respectively. The reactivity can be expressed in terms of k_{eff} by definition, so one would get

$$\Delta\rho = \frac{k'_{eff} - 1}{k'_{eff}} - \frac{k_{eff} - 1}{k_{eff}} = \frac{1}{k_{eff}}\left(1 - \frac{k_{eff}}{k'_{eff}}\right). \tag{2}$$

The main manifestation of the poisoned reactor is seen as an increase in parasitic absorption of thermal neutrons, meaning that thermal utilization *f*-factor is diminishing. In that sense, the ratio of unpoisoned-to-poisoned k_{eff} factors is equivalent to the ratio of *f*-factors as

$$\frac{k_{eff}}{k'_{eff}} = \frac{f}{f'} = \frac{\Sigma_{aT} + \Sigma_{aP}}{\Sigma_{aT}}\,, \tag{3}$$

where macroscopic absorption cross sections are Σ_{aP} for poisons and Σ_{aT} for all nuclide absorbers before poisoning occurred. Since operating reactor will be near critical condition ($k_{eff} \approx 1$), the reactivity decrease will be defined by the ratio of thermal neutrons absorbed in the poisons to neutrons absorbed in all of the absorbers of unpoisoned reactor:

$$\Delta\rho = 1 - \frac{f}{f'} = -\frac{\Sigma_{aP}}{\Sigma_{aT}}. \tag{4}$$

This general equation is a staring point for further analyses presented in the rest of the paper, organized as follows. Chapter 2 gives analytical solution to ^{135}Xe poisoning problem and reactivity change, where thermal utilization *f*-factor becomes integral part of the solution equations. The Wigner-Seitz method for calculating the *f*-factor is presented in Chapter 3 using the thermal neutron diffusion in cylindrical geometry. Short overview of the programming details is presented in Chapter 4, leading to a practical database of *f*-factors and ^{135}Xe poisoning results for user-defined unit cell and reactor parameters. The application and training of PINNs on generated database is presented in Chapter 5 with comparison to deterministic C-language based results. The conclusions with future work are presented in Chapter 6 while the referenced literature is given at the end of the paper.

2 XENON POISONING

The extremely large absorption cross section (2.65 million barns) for thermal neutrons is what separates ^{135}Xe from many fission products, and other factor is its high share: only 0.3% fissions of ^{235}U will directly generate ^{135}Xe, while most part is coming from radioactive decay of tellurium ^{135}Te, which is formed in 6.1% of all fissions. The ^{135}Te is short lived (19 sec) with a decay scheme leading to stable barium isotope:

$$^{135}\mathrm{Te} \xrightarrow{19\ \mathrm{sec}} {}^{135}\mathrm{I} \xrightarrow{6.7\ \mathrm{hrs}} {}^{135}\mathrm{Xe} \xrightarrow{9.2\ \mathrm{hrs}} {}^{135}\mathrm{Cs} \xrightarrow{2.3\cdot10^{6}\ \mathrm{yrs}} {}^{135}\mathrm{Ba} \tag{5}$$

Since 19 sec is negligible to 6.7 hrs, it is justified to assume how ^{135}I is formed directly in fissions, and this assumption simplifies the following iodine balance equation:

$$\frac{dI}{dt} = -\lambda_I I - \sigma_I \phi I + 0.061\Sigma_f \phi, \tag{6}$$

where I is the iodine volume concentration, λ_I is the iodine decay constant and σ_I is the iodine absorption cross section for thermal neutrons. If one compares numerical values of constants, then another simplification is possible, to dismiss middle term due to small σ_I. The steady-state iodine concentration if found by setting dI/dt =0, where steady-state flux ϕ_0(n/cm^2/s) is introduced:

$$I_0 = 0.061\frac{\Sigma_f}{\lambda_I}\phi_0. \tag{7}$$

Repeating the same procedure, one would get the balance equation for ^{135}Xe as:

$$\frac{dXe}{dt} = -\lambda_{Xe} Xe - \sigma_{Xe}\phi Xe + \lambda_I I + 0.003\Sigma_f \phi. \tag{8}$$

The first two terms give xenon loss due to radioactive decay and large thermal neutron absorption, while the last two terms give xenon production from iodine decay and by ^{235}U fission. The equilibrium xenon concentration Xe_0 (#/cm^3) can be found as dXe/dt = 0, and by inserting the iodine equilibrium concentration we obtain:

$$Xe_0 = \frac{\lambda_I I_0 + 0.003\Sigma_f \phi_0}{\lambda_{Xe} + \sigma_{Xe}\phi_0} = \frac{0.064\Sigma_f \phi_0}{\lambda_{Xe} + \sigma_{Xe}\phi_0}. \tag{9}$$

We are now able to express the reactivity change from Eq. (4) caused by the equilibrium xenon poisoning as:

$$\Delta\rho = -\frac{Xe_0\sigma_{Xe}}{\Sigma_{aT}} = -\frac{0.064\Sigma_f \phi_0 \sigma_{Xe}}{\Sigma_{aT}(\lambda_{Xe} + \sigma_{Xe}\phi_0)}. \tag{10}$$

The eta-factor η or the average number of fission neutrons emitted per thermal neutron absorbed in fuel can be utilized to express the ratio $\Sigma_f / \Sigma aT = (\eta f)/\nu$, where ν is the average number of emitted fission neutrons (~2.42). The η-factor depends only on the nuclear fuel type and not on the moderator or spatial arrangement of the fuel inside it. However, the reactivity change is dependent on fuel geometrical arrangement, i.e. on the unit cell geometry as seen through the *f*-factor, which will be explicitly modelled in our calculation:

$$\Delta\rho = -0.064\frac{\eta}{\nu}\frac{f\phi_0\sigma_{Xe}}{\lambda_{Xe}+\sigma_{Xe}\phi_0}. \quad (11)$$

A special case of significant practical importance is sudden reactor shutdown (scram or trip), resulting in a high-power level change, where the neutron flux is quickly brought to zero. The solution to Eq. (8) is now given as

$$Xe(t) = \frac{\lambda_I}{\lambda_{Xe}-\lambda_I} I_0(e^{-\lambda_I t} - e^{-\lambda_{Xe} t}) + Xe_0 e^{-\lambda_{Xe} t}, \quad (12)$$

where $t = 0$ is the reactor shutdown moment with initial equilibrium concentrations of xenon Xe_0 and iodine I_0. Since the ^{135}I has a half-life smaller than ^{135}Xe, after the shutdown xenon will accumulate and thus lower the reactor reactivity as the time-dependent function:

$$\Delta\rho(t) = -\frac{\sigma_{Xe}Xe(t)}{\Sigma_{aT}} = -\frac{\sigma_{Xe}\phi_0 f\eta}{\nu}\left[\frac{0.061}{\lambda_{Xe}-\lambda_I}(e^{-\lambda_I t} - e^{-\lambda_{Xe} t}) + \frac{0.064}{\lambda_{Xe}+\sigma_{Xe}\phi_0}e^{-\lambda_{Xe} t}\right]. \quad (13)$$

This negative reactivity due to xenon can be several times higher compared to steady-state values prior to reactor shutdown, especially for high neutron flux values. For example, if the stationary neutron flux was above $1\cdot10^{14}$ n/cm^2/s and the reactor has reactivity reserve of ρ_r, then after the shutdown there is a time period known as the reactor deadtime (or xenon pit) where $\Delta\rho(t) > \rho_r$ and in which reactor cannot be restarted [1]. This operational problem is important only in thermal neutron reactors, due to the large absorption cross section of ^{135}Xe, while intermediate and fast reactors are not affected. The maximum value of negative reactivity is reached about 11 h after the shutdown while the time of return to stationary value is about 40 h [1].

Several important operational information can be obtained from the time dependent xenon concentration. One of them is time to reach the maximum negative reactivity from Eq. (12) as:

$$t_m = \frac{1}{\lambda_I - \lambda_{Xe}}\ln\left[\frac{\lambda_I}{\lambda_{Xe}}\left(1+1.04\frac{\lambda_I-\lambda_{Xe}}{\lambda_{Xe}+\sigma_{Xe}\phi_0}\right)\right]. \quad (14)$$

The other one is relative ratio of time-dependent concentration $Xe(t)$ to equilibrium value of xenon Xe_0, providing information about time necessary to reach a steady-state value as:

$$\frac{Xe(t)}{Xe_0} = 1 + 0.953\left[\left(\frac{\lambda_I}{\lambda_{Xe}-\lambda_I+\sigma_{Xe}\phi_0} - 0.0049\right)e^{-(\lambda_{Xe}+\sigma_{Xe}\phi_0)t} - \left(\frac{\lambda_{Xe}+\sigma_{Xe}\phi_0}{\lambda_{Xe}-\lambda_I+\sigma_{Xe}\phi_0}\right)e^{-\lambda_I t}\right]. \quad (15)$$

The change in xenon concentration will affect the reactivity for every reactor power level adjustment, being more pronounced at high power changes during a shorter time interval. This can lead to xenon oscillations and cyclic shift in axial power distribution of the reactor, burdening the core materials with temperature cycling which may led to premature materials failure.

3 THERMAL UTILIZATION FACTOR FOR HETEROGENEOUS CELL

It was already shown that *f*-factor is included in analytical solution to negative reactivity change due to ^{135}Xe poisoning, so this section gives solution to the *f*-factor using Wigner-Seitz [1] approach for heterogeneous unit cell description. The thermal neutron flux depression inside the uranium rod and determination of average values in fuel and moderator will be based on neutron

diffusion theory. The substitution of the square unit cell (side *a*) with an equivalent round one (radius $r = \sqrt{a^2/\pi}$) of the same area will simplify analysis in the cylindrical system resulting only in radially dependent neutron flux. Even though the theoretical conditions to use diffusion theory are not met for this problem, the empirical knowledge shows a satisfactory level of agreement.

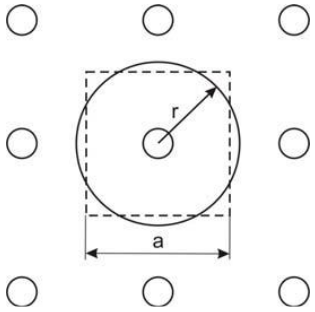

Figure 1: The square unit cell (side *a*) relative to equivalent round cell (radius *r*)

In the following analysis, r_f is the nuclear fuel radius and r_m is the moderator radius, both related to equivalent unit cell in Figure 1 (other materials are disregarded). The thermal neutron diffusion equation inside the fuel rod has a zero-source term since fuel is source of fission neutrons, while moderator produces thermalized neutrons

$$D_f \nabla^2 \phi_f - \Sigma_{af} \phi_f = 0 \Rightarrow \nabla^2 \phi_f - K_f^2 \phi_f = 0, \tag{16}$$

where K_f^2 is the inverse value of squared diffusion length of thermal neutrons in the fuel defined as $L_f^2 = D_f / \Sigma_{af}$. The neutron diffusion equation for moderator region is similar

$$\nabla^2 \phi_m - K_m^2 \phi_m + \frac{Q}{D_m} = 0, \tag{17}$$

where K_m^2 is the inverse value of squared diffusion length of neutrons ($L_m^2 = D_m / \Sigma_{am}$) in moderator and Q(n/cm^3/s) is thermal neutron source inside the moderator. The procedure to solve these equations, giving the neutron flux distribution in the fuel rod and moderator, is quite tedious with Laplace operator being expressed in the cylindrical system, resulting in modified Bessel functions I_0, I_1, K_0 and K_1. The boundary conditions demand continuity of the neutron flux and neutron current at fuel-moderator interface ($r=r_f$) and zero-current at equivalent cell radius ($r=r_m$), meaning no net neutron transport between neighbouring cells of the fuel element.

The thermal utilization factor solution $1/f$ is expressed in the closed form as [1]

$$\frac{1}{f} = \frac{\Sigma_{am} V_m}{\Sigma_{af} V_f} F(K_f, r_f) + E(K_m, r_m, r_f), \tag{18}$$

where cylindrical fuel rod lattice functions *E* and *F* are defined as

$$F(K_f, r_f) = \frac{K_f r_f I_0(K_f r_f)}{2 I_1(K_f r_f)}, \tag{19}$$

$$E(K_m, r_m, r_f) = \frac{K_m (r_m^2 - r_f^2)}{2 r_f} \left[\frac{I_0(K_m r_f) K_1(K_m r_m) + K_0(K_m r_f) I_1(K_m r_m)}{I_1(K_m r_m) K_1(K_m r_f) - K_1(K_m r_m) I_1(K_m r_f)} \right], \tag{20}$$

with volume per unit length of the fuel $V_f = \pi(r_f^2)$ and the moderator $V_m = \pi(r_m^2 - r_f^2)$.

It should be noted that the F function depends only upon the diffusion length and the fuel radius, while E function depends upon the diffusion length and the inner and outer radius of the moderator. The F function is equal to the ratio of the flux at the fuel surface to the average value of the flux within the fuel rod. The interpretation of the E function requires more work and can be stated as [1]: per neutron absorbed in the fuel rod, the E - 1 equals the number of neutrons absorbed in the moderator in excess of the number which would be absorbed with a constant flux corresponding to the fuel surface flux value. Consequently, $E - 1$ is generally small while F may be much greater than unity, implying how the F function is mainly responsible for the decrease in the f-factor. The approximate expressions for the F and E function using series expansion can be found in [2]. One should bear in mind limitations of the diffusion theory for describing neutrons in highly absorbing medium such as uranium fuel, resulting in neutron flux depression, so better result can be obtained by using transport corrections to K_f for UO_2 matrix fuel such as [2]:

$$\frac{K_f}{\Sigma_{af}+\Sigma_{sf}} = \tanh\left(\frac{K_f}{\Sigma_{sf}}\right), \tag{21}$$

where absorption and scattering cross sections for thermal neutrons are needed. In case of homogeneous mixture of fuel and moderator, the f-factor loses its spatial feature and depends only on absorption cross sections of the fuel and the moderator as:

$$f = \frac{\Sigma_{af}}{\Sigma_{af}+\Sigma_{am}}. \tag{22}$$

4 XENON POISONING AND F-FACTOR PROGRAMING DETAILS

The C-programming language [3][4][5] was used for coding numerical routines which solve the heterogeneous f-factor as a function of unit cell geometry and material compositions, together with the ^{135}Xe poisoning problem. The modular structure of the program includes several routines or solvers for different objectives, such as number densities mixer depending on fuel enrichment and material density, modified Bessel functions (I_0, I_1, K_0, K_1), analytic and approximate solution to F and E lattice functions, K_f transport correction, etc. Using the terminal window shown in Figure 2, the user selects typical values for the unit cell dimensions and materials, with default (industrial) values given in square brackets.

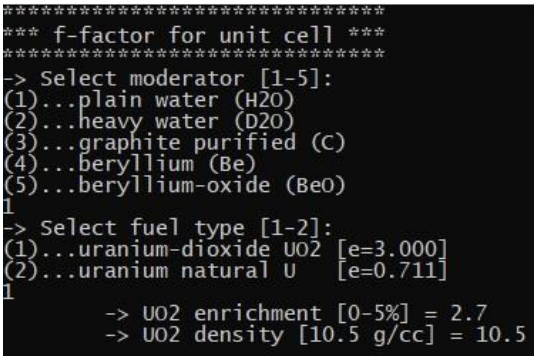

Figure 2: Selection of unit cell fuel and moderator

After the selection of standard moderator (water, heavy water, reactor-grade graphite, beryllium, or beryllium-oxide), the user selects uranium fuel type which can be metallic or ceramic UO_2. The fuel enrichment level up to max 5% and fuel density (in g/cm^3) are entered lasty in command prompt window.

After that, the nuclear data for the fuel and the moderator (at 0.025 eV) are calculated and printed in the terminal window (Figure 3): macroscopic cross sections (absorption and scattering) and thermal neutron diffusion parameters defined in the previous text (L, D, K).

```
Moderator data @ 0.025 eV:
* absorption xs  Sig_am = 0.019700 1/cm
* diffusion length   Lm = 2.849882 cm
* diffusion const..  Dm = 0.160000 cm
* 1/diffusion length Km = 0.350892 1/cm


Fuel data @ 0.025 eV:
* absorption xs  Sig_af = 0.497552 1/cm
* diffusion length   Lf = 2.805000 cm
* diffusion const..  Df = 3.914753 cm
* 1/diffusion length Kf = 0.356506 1/cm
```

Figure 3: The neutron diffusion parameters print-out

Figure 4 shows input data for the square unit cell geometry (cell side and fuel radius) from which the equivalent unit cell data is calculated, together with region volumes per cm of the cell length. After that, the comparison (absolute and relative) of homogeneous vs. heterogenous thermal utilization f-factor is printed.

```
Square unit cell [Westinghouse]:
-> cell side a [1.2598 cm] = 1.26
-> fuel radius rf [0.3922 cm] = 0.39
-> gap radius rg [0.4000 cm] = 0.40

Thermal utilization f-factor:
        |---Homogen.cell = 0.961914
        |---Wigner-Seitz = 0.910829
        |---Newmarch cor = 0.912823

Relative error het-to-hom:
        |---Wigner-Seitz = -5.31 %
        |---Newmarch cor = -5.10 %
```

Figure 4: Unit cell geometry input with f-factor comparison

Besides Wigner-Seitz method, the flux solution with modified boundary conditions by Newmarch [6] was also programmed for inclusion of the gap layer between the fuel and the moderator which will flatten the neutron distribution and thus reduce excess absorption of neutrons in the moderator. Finally, the values of lattice functions F and E from Eq. (19) and (20) are printed, together with approximative series expansion retaining only first few terms (Figure 5). In this way the user can gain information about the importance of unit cell description regarding the geometrical configuration of fuel and moderator materials.

```
-------- Lattice functions -------
F(0.36,0.39) - 1 = 0.002414
E(0.39,0.71,0.35) - 1 = 0.005723
f_het = 0.910829
---------------------------------

-------- Series expansion --------
F(0.36,0.39) - 1 = 0.002414
E(0.39,0.71,0.35) - 1 = -0.004656
f_het = 0.919521
---------------------------------
```

Figure 5: Printout of the lattice functions F and E

Using modular program structure, the heterogeneous f-factor, being a corrective term in the analytic solution of ^{135}Xe poisoning equations, is transferred to the xenon program solver. The xenon module has several options to calculate equilibrium and dynamical ^{135}Xe concentration (and

reactivity), reactor deadtime, and time to reach maximum negative reactivity. The calculated data is printed in the terminal window as a default option but can be easily exported into external file. The numerical methods of Press et al [7] were implemented in our C-program for modified Bessel functions and root finding of nonlinear equations.

The deterministic quantification of the *f*-factor and xenon poisoning for a square unit cell and several operating reactor parameters served for generating a database or "truth table" which was used for training and validating physics-informed neural network algorithms (PINNs). The obtained results are presented in the following section.

5 PHYSICS-INFORMED NEURAL NETWORKS

Physics-Informed Neural Networks (PINNs) were introduced by M. Raissi and collaborators [8] as a method for solving differential equations using deep learning. PINNs represent a class of neural networks from which they differ by the incorporation of known physical laws directly into the training process. Unlike traditional data-driven approaches, PINNs do not rely solely on observational or experimental data, instead, they integrate prior physical knowledge in the form of partial differential equations (PDEs), initial, and boundary conditions. The neural network acts as a universal function approximator of the solution to the problem.

The training process is essentially an optimization problem in which the network parameters are determined by minimizing a composite loss function [8]. In the general PINN framework, for a neural network $\phi_\theta(r)$ with trainable parameters θ (weights and biases), one should first define the physical residual $R(r)$ as the pointwise departure from the governing differential equation evaluated at the network output rather than the true solution. For the present problem, the residuals formed based on Eq. (16) and (17) specific to the fuel and moderator regions are:

$$R_f(r) = D_f \nabla^2 \phi_\theta(r) - K_f^2 \phi_\theta(r), \text{ with } r \in \left[0, r_f\right] \tag{23}$$

$$R_m(r) = D_m \nabla^2 \phi_\theta(r) - K_m^2 \phi_\theta(r) + \frac{Q}{D_m}, \text{ with } r \in \left[r_f, r_m\right]. \tag{24}$$

The composite loss function $L(\theta)$ is then constructed, in general, as a weighted sum of mean squared residuals over collocation points sampled randomly from the domain (N_f points in fuel, N_m points in moderator), along with squared penalties enforcing the boundary and interface conditions. In this problem it takes the form:

$$\begin{aligned} L(\theta) = {} & \frac{\lambda_f}{N_f} \sum_j R_f^2(r_j) + \frac{\lambda_m}{N_m} \sum_j R_m^2(r_j) + \lambda_1 \left(\phi_\theta^f(r_f) - \phi_\theta^m(r_f) \right)^2 + \\ & \lambda_2 \left(D_f \frac{d\phi_\theta^f(r_f)}{dr} - D_m \frac{d\phi_\theta^m(r_f)}{dr} \right)^2 + \lambda_3 \left(\frac{d\phi_\theta^m(r_m)}{dr} \right)^2 + \lambda_4 \left(\phi_\theta(0) - 1 \right)^2 \end{aligned} \tag{25}$$

To each term a weight coefficient λ_i is assigned which controls the relative influence of each contribution during training. The weights are problem-specific and are determined empirically, as no general rule for their optimal selection exists. The minimization of $L(\theta)$ is carried out by standard gradient-based optimization common to all neural network training [9]:

$$\theta_{k+1} = \theta_k - \eta \nabla_\theta L(\theta_k), \tag{26}$$

where η is the learning rate and $\nabla_\theta L(\theta_k)$ is the gradient of the loss with respect to the network parameters computed with automatic differentiation. In this paper, no experimental or synthetic data is used, so the data term carries zero weight in the loss function.

Compared to traditional numerical methods such as finite difference or finite element approaches, PINNs do not require explicit discretization of the spatial domain. Derivatives are evaluated using automatic differentiation, enabling direct enforcement of the governing equations in their continuous form.

5.1 PINN for thermal neutron flux calculation

Based on the unit cell geometry defined in Section 3 and using data presented in Figures 2-5, the diffusion equations (16) and (17) are directly solved using the PINN approach, yielding a continuous function that describes the neutron flux across the entire cell. Two separate neural networks are created – one for the fuel region and one for the moderator region, each consisting of three hidden layers of 64 neurons with hyperbolic tangent activation functions. The loss function enforces the governing PDE in each region, flux and current continuity at the interface, zero current at the outer cell boundary, and a normalization condition $\phi(0) = 1$ at the fuel rod centre. Since the thermal neutron source term Q in equation (17) is not explicitly known (as it is not needed in the prior calculation), a value consistent with the chosen flux normalisation is assumed, and a sensitivity analysis confirms that variation of this parameter over several orders of magnitude has negligible impact on the resulting *f*-factor which is expected from the analytical solution structure.

In this paper, no experimental or synthetic data is used so it does not have a contribution in the loss function, or its weight is equal to zero. The weight coefficients were determined empirically through iterative experimentation, which is a known challenge in PDE-driven PINN formulations. No general rule exists for optimal weight selection, and it mostly depends on the context of the problem. Network parameters are optimised in two phases. In the first phase, the Adam optimiser [9] is used for 20 000 epochs with an initial learning rate of 10^{-3} and cosine annealing schedule, requiring approximately 9 minutes and 39 seconds. In the second phase, the L-BFGS optimiser [10] with strong Wolfe line search conditions is applied for 200 iterations, requiring an additional 46 seconds. The total computational time is approximately 10 minutes and 25 seconds on a laptop equipped with an AMD Ryzen AI9 HX 370 processor and 32 GB of RAM. Once trained, the network evaluates the flux at any spatial point instantaneously.

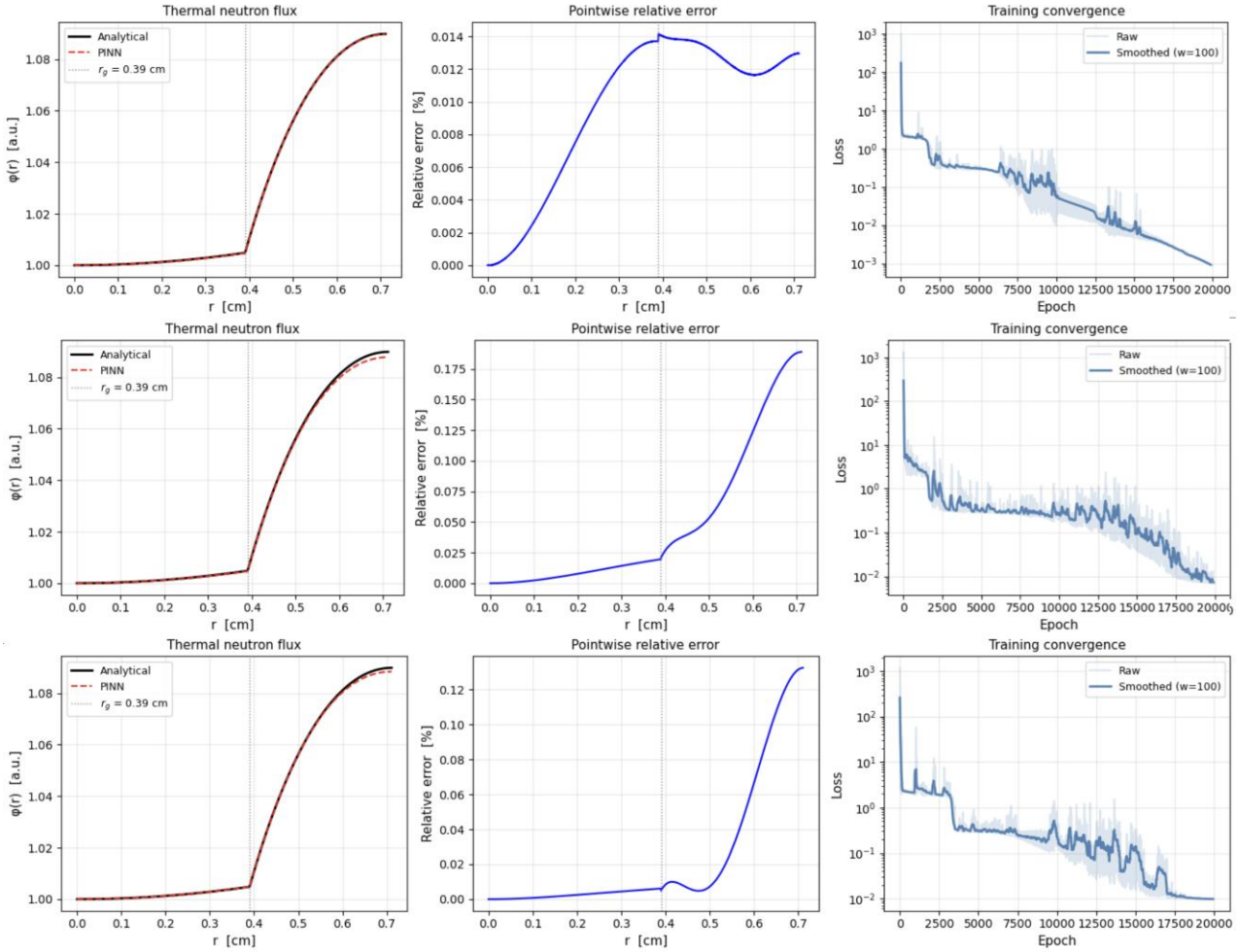

Figure 6: Thermal neutron flux comparison, pointwise relative error, and training convergence for three independent PINN training runs.

The training was repeated three times with different random seeds to demonstrate the consistency of the PINN result and to visualise statistical variability inherent to stochastic network initialization. The flux comparison, pointwise relative error, and training convergence for all three runs are shown in Figure 6 and discussed below.

The PINN neutron flux is compared to the analytical Bessel function solution in column 1 of Figure 6. The flux exhibits the expected physical behaviour: a nearly flat profile in the fuel with approximately 0.4% variation between the rod centre and the rod surface, followed by a rising in the moderator reaching a maximum at boundary, consistent with the reflective boundary condition and the presence of the thermal neutron source.

The pointwise relative error between the PINN and analytical flux is shown in column 2 of Figure 6. The error profile varies between runs because of the stochastic training initialisation but remains below 0.2% across all three runs and throughout the entire domain. This confirms that while the specific solution found by the network differs between runs, the accuracy is consistently maintained within an acceptable range.

The training convergence is shown in column 3 of Figure 6. All three runs exhibit a clear monotonically decreasing loss throughout the training process, confirming that the optimisation converges reliably regardless of the random initialisation. The statistical differences between runs are visible but do not affect the quality of the result.

5.2 Application to *f*-factor and reactivity change

The thermal utilization factor f is computed directly from PINN flux using its standard definition as the ratio of neutron absorption in the fuel to total neutron absorptions in the unit cell:

$$f = \frac{\Sigma_{af}\bar{\phi}_f V_f}{\Sigma_{af}\bar{\phi}_f V_f + \Sigma_{am}\bar{\phi}_m V_m}. \tag{27}$$

The integrals are evaluated numerically from the trained network output. Table 1 compares the PINN result against the Wigner-Seitz Figure 4 reference and the homogeneous approximation defined in Eq. (22). Despite the existing moderator flux error, the PINN obtained *f*-factor agrees with the reference to within 0.009% for all three runs. The robustness is a consequence of a physical feature of the problem: the macroscopic absorption cross section ratio of fuel vs. moderator (~25) is a dominant value in the calculation, suppressing the contribution of flux errors. In other words, a constant flux (homogeneous solution) provides a correct result up to two significant digits with an overestimation of 5.6%, meaning that the PINN solution only becomes satisfactory if it remains consistent with the Wigner-Seitz solution for more than said two digits, which, as seen in Table 1, it does.

Table 1: Thermal utilization *f*-factor comparison

Method	f - factor	Error
Homogeneous, Fig. 4	0.961914	5.6000%
Wigner-Seitz, Fig. 4	0.910829	reference
PINN - Run 1	0.910749	0.0088%
PINN - Run 2	0.910824	0.0005%
PINN - Run 3	0.910790	0.0043%

The PINN derived *f*-factor (from Run 2) is subsequently inserted into equation (11) to compute the equilibrium xenon reactivity change $\Delta\rho$, as well as equation (13) to compute the time-dependent reactor reactivity change $\Delta\rho(t)$. Table 2 presents results using a steady-state neutron flux of $\phi_0 = 5 \cdot 10^{13}$ neutrons/cm²/s.

Table 2: Equilibrium xenon reactivity change

Method	f - factor	$\Delta\rho$	Error
Homogeneous	0.961914	-0.041245	5.61%
Wigner-Seitz	0.910829	-0.039054	reference
PINN – Run 2	0.910824	-0.039054	<0.01%

The PINN-derived reactivity estimate is in excellent agreement with the Wigner-Seitz reference, confirming that the accuracy of the *f*-factor computation is sufficient for practical reactor physics calculations.

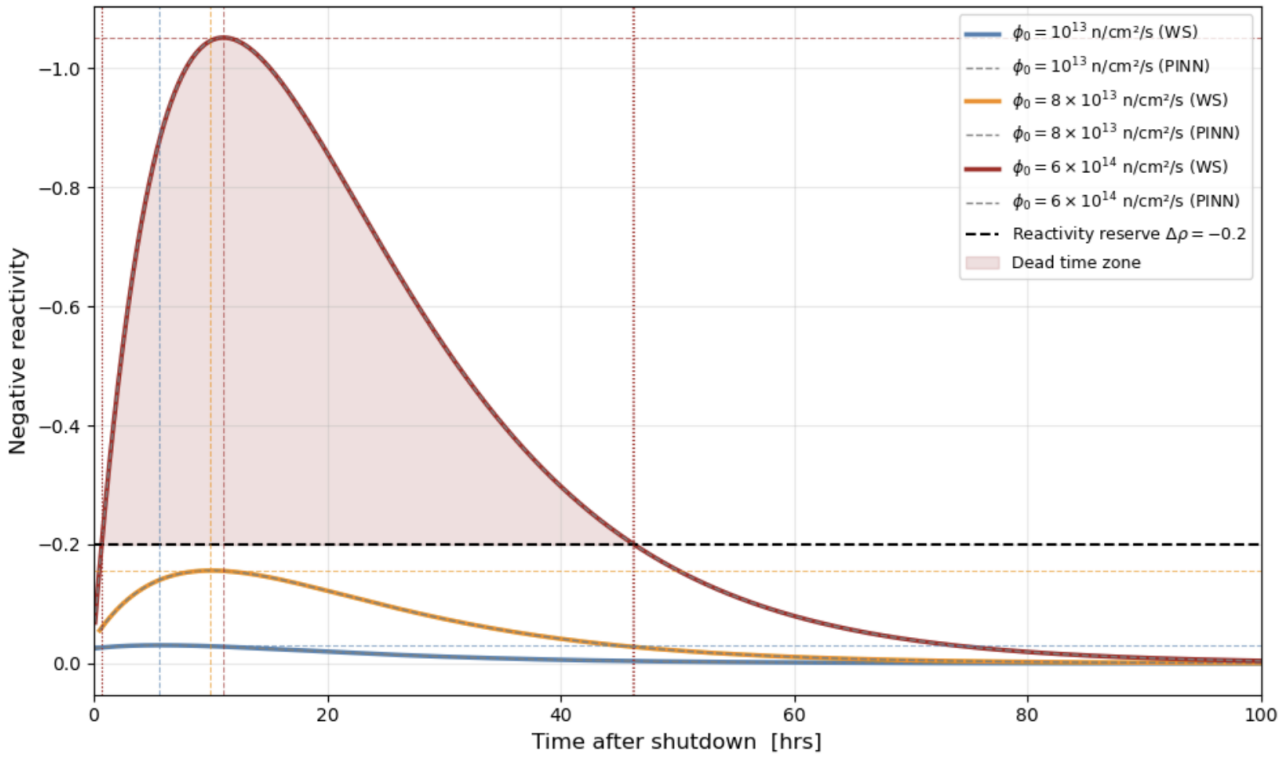

Figure 7: Xenon-135 buildup after shutdown for PINN and Wigner-Seitz *f*-factors

The time-dependent ^{135}Xe reactivity change following reactor shutdown is examined for three steady-state neutron flux levels: $\phi_0 = 10^{13}$, $8 \cdot 10^{13}$, and $6 \cdot 10^{14}$ n/cm²/s. The results are presented in Figure 7, where solid lines represent the Wigner-Seitz reference and dashed lines represent the PINN outcome. For all three fluxes, the two curves are indistinguishable on the scale of the figure, confirming that the PINN *f*-factor produces results fully consistent with the reference values. At the highest steady-state flux of $\phi_0 = 6 \cdot 10^{14}$ n/cm²/s, the xenon pit deepens significantly and exceeds the reactivity reserve almost immediately after shutdown at $t \approx 0.7$ hours. The reactor remains in dead time zone until $t \approx 46.3$ hours. The specific numerical details of the figure are secondary to its broader significance: the results obtained using the PINN-derived *f*-factor are fully consistent with the expected physical behaviour, as demonstrated by direct comparison to referenced values [1].

6 CONCLUSION

The thermal neutron utilization *f*-factor for a heterogeneous PWR fuel cell in the Wigner-Seitz approximation was successfully computed using a physics-informed neural network trained solely on the governing neutron diffusion equations and boundary conditions, without the use of experimental or synthetic measurement data. Two separate networks were employed for the fuel and moderator regions. The PINN reproduced the *f*-factor to within 0.0005% of the reference and the result was shown to be consistent across multiple independent training runs, confirming the robustness of the approach.

The *f*-factor was found to be insensitive to moderate pointwise flux errors, owing to the large fuel-moderator absorption cross section ratio and the smoothing effect of spatial integration. This property makes the PINN approach particularly suitable for computing integral reactor physics quantities even when the underlying flux solution carries local errors. The loss function weight coefficients were determined empirically, which is a known limitation of PDE-only PINNs. It is

useful to note that the incorporation of sparse measurement data, such as flux detector readings, would provide natural anchoring of the solution and reduce sensitivity to weight selection.

Future work could apply the validated method to unit cell geometries for which analytical solutions do not exist, such as non-circular fuel cross sections or clustered rod assemblies. The present results establish that the PINN approach reproduces both the neutron flux distribution and the derived reactor physics quantities with accuracy suitable for engineering applications, providing a mesh-free and data-efficient alternative to conventional deterministic codes for reactor cell calculations.

REFERENCES

[1] J.R. Lamarsh, Introduction to Nuclear Reactor Theory, Addison-Wesley Publishing Company, USA, 1972.

[2] D. Feretić, Uvod u nuklearnu energetiku, Školska knjiga, Zagreb, 1992.

[3] B.W. Kernighan, D.M. Ritchie, The C Programming Language, 2nd edition, Prentice Hall PTR: Saddle River, NJ, USA, 1988.

[4] The GNU C Compiler. Available online: https://gcc.gnu.org/ (accessed on 26 March 2026).

[5] The GNU C Language Intro and Reference Manual. Available online: https://www.gnu.org/software/c-intro-and-ref/manual/ (accessed on 26 March 2026).

[6] A.M. Weinberg, E.P. Wigner, The Physical Theory of Neutron Chain Reactors, University of Chicago Press, USA, 1959.

[7] W.H. Press, S.A. Teukolsky, W.T. Vetterling, B.P. Flannery, Numerical Recipes in C – The Art of Scientific Computing, 2nd Edition, Cambridge University Press, New York, USA, 1992.

[8] M. Raissi, P. Perdikaris, G.E. Karniadakis, Physics-informed neural networks: A deep learning framework for solving forward and inverse problems involving nonlinear partial differential equations, Journal of Computational Physics, Vol. 378, pp. 686–707, 2019.

[9] D.P. Kingma, J. Ba, Adam: A Method for Stochastic Optimization, In Proceedings of the 3rd International Conference on Learning Representations (ICLR), San Diego, CA, USA, 2015.

[10] D.C. Liu, J. Nocedal, On the Limited Memory BFGS Method for Large Scale Optimization, Mathematical Programming, Vol. 45, pp. 503–528, 1989.